068 APPLICATIONS OF COHERENCES OF ULTRASOUNDS AND LOW FREQUENCY WAVES.

C. Sumi, Y. Ishii, N. Yamazaki, Y. Hirabayashi.*

Sophia University, 7–1, Kioi–cho, Chiyoda–ku, Tokyo 102–8554 JAPAN.

Submitted for publication in final form: October 2, 2012.

Introduction

The developments of useful ultrasound (US)–echo–based tissue displacement measurement methods and beamforming methods increase the medical diagnosis applications of displacement/strain/mechanical property measurements (e.g. various blood flow, motions of the heart, liver, breast etc.). For instance, our previously developed combination of the multidimensional autocorrelation method (MAM) and lateral modulation (LM) methods (e.g. [1-5]) or single beam methods (e.g. [5-8]) resulted in accurate two– or three–dimensional displacement vector/strain tensor measurements.

Our developed LMs can be achieved only through the use of superposed, crossed, steered beams. Specifically this involves the use of superposed multiple steered beams with different steering angles using the multiple transmission method (MTM) (e.g., [1,3,4,9,10]), or which are synthesized from a set of received echo data using the multidirectional synthetic aperture (SA) method (MDSAM) (e.g., [1,3,4,9,10]) [11]. For high speed scanning, simultaneous or successive transmissions of plural plane waves [1,3,4,11] can also be performed. Multiple transducers can also be used. It is also shown that the combination of the new beam angle (BA) method [5] with one-dimensional autocorrelation method for the multiple crossed beams (MCB) method with non-superimposed or separated beams [4,7,9,10] obtained from MTM or MDSAM is theoretically equivalent to MAM and LM. LM also permits echo imaging with almost the same lateral resolution as the axial resolution [1,3,8]. Simple single beam methods (i.e., a non-steering method or a steering angle method [ASTA]) are particularly effective when using the spectral frequency division method (SFDM) [5-8]. The new beam angle (BA) method [5] can also be used for a lateral displacement measurement and yields a more accurate measurement than the lateral Doppler method [7]. In addition to the application of beam steering, proper apodization should be performed for the respective spherical focusing and plane wave transmissions (e.g., [1,3,4,8,12]). For the axial, lateral and displacement vector measurements, over-determined systems were generated for non-steering, and one or multiple steering angle LMs and ASTAs, i.e., by performing superposition and/or division of spectra (e.g., [11,13]).

We have also been developing combined digital US diagnosis/treatment systems (e.g. [9-11,14-16]), in which (i) diagnostic US echography can be performed, (ii) a high intensity focus US treatment can also be performed for echo–based and/or radiation–force–based diagnostic measurement/imaging, as well as the combination used with diagnostic ultrasounds, (iii) radiation force can also be used for echo–based measurement/imaging. In the systems, the above-mentioned beamforming and measurement/imaging can also be performed simultaneously or successively with the generation of thermal and/or mechanical sources (special beamformers are equipped with). We are also interested in the applications on tissue/cellular engineering (e.g., [17-19]). Recently, a radiation force imaging (ARFI) is used as a diagnosis modality [20-22].

Useful applications of coherences of ultrasounds and low frequency waves can be performed using such systems. Specifically, coherent superpositions of spectra or echo signals and/or the spectral frequency divisions are performed with weighting [11,23,24] for yielding (1) high spatial resolution imaging/treatment, (2) accurate displacement vector/strain tensor measurements, (3) desired mechanical and/or thermal sources, (4) desired low frequency deformations or low frequency wave propagations and (5) accurate temperature measurements, etc. Interferences of US or low frequency beams/waves are properly used for synthesizing new beamforming/wave parameters such as a wavefront, a propagation direction, a steering angle, frequencies, bandwidths, focuses etc. Quasi–beams/quasi-waves can also be generated by signal processing (i.e., not physically generated ones). Using several sources also allows the generation of various propagation directions of low frequency waves/various deformation fields. For instance, an anisotropic measurement is allowed. External compressions/vibrations can also be used. Temporal and/or spatial filtering can also be performed in the frequency domain to change beam/wave properties or separate signals or waves (e.g. plural crossed beams/waves, and mechanical and thermal strains, etc.). In our target systems, parallel processing is performed on the same received raw echo data to yield proper echo data for the respective purposes. In this report, the results obtained are shown together with speckle reduction achieved by incoherent superposition of horizontally and/or vertically divided or superposed spectra for one or multiple LMs and ASTAs (i.e., over-determined ones). The results are compared with non-steering with such spectra divisions [8,11,13] and SonoCT obtained using MDSAM [11].

Methods

For spectra obtained using LMs, ASTAs and non-steering, superposition and/or division, weighting, multidimensional super-resolution and filtering were performed. The first point was the evaluation of

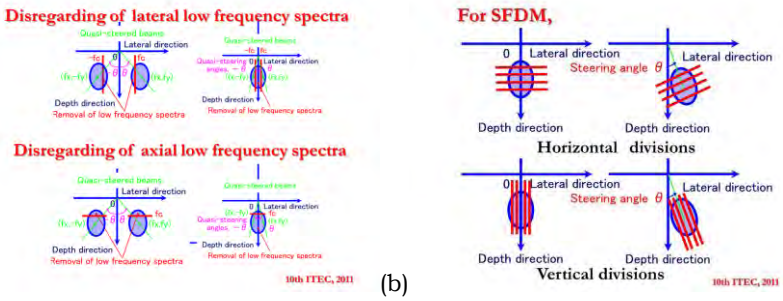

(a) (b)

Figure 1. (a) Disregarding of low lateral and axial frequency spectra [8,13,24]. Quasi-beams are generated. See the processing in detail by referring to ref. [8] (particularly, the lateral processing). The boundaries (red lines) for the disregarding low frequency spectra can also be set in the directions of generated beams and the orthogonal directions to the beam directions or curvedly (i.e., not on the orthogonal coordinate axes). (b) Spectral frequency divisions (SFDMs) for LM, ASTA and non-steering [8,13,24].

signal–to–noise ratios (SNRs) of generated spectra (agar phantom experiments). This was performed in a frequency domain by the evaluation of the positions of signal spectra moments and a distribution of signal spectra together with the stochastic assumption of noise spectra (i.e., random noise) [13]. See Figures 4 and 5A in ref. [8]. This led to disregarding low axial frequency spectra (see Figure 1a, a slide presented at the 10th conf. [13]) for increasing the displacement calculation speed [24]. The disregarding was particularly effective for parabolic apodization, because the apodization yields a low SNR in a low frequency range. Also see in refs. [8,13], the effectiveness of the low lateral frequency spectra (Figure 1a), i.e., the increase in a displacement measurement accuracy for single beam scanning and LM scanning with rectangular apodization; and the generation of quasi-LM echo imaging through the single beam scanning. The Ziv-Zakai Lower Bound [25,26] and/or energy estimated for the obtained spectra was used to increase the measurement accuracy using such over-determined systems (experiment) [24] (see the applications of SFDM in Figure 1b, whereas the schematic about multiple beams are omitted). Such weighting can also be performed *a posteriori* at respective measurement positions [27], and will be reported in detail elsewhere.

The second point was to properly perform the evaluations of generated point spread functions (PSFs), and mechanical sources and thermal sources (i.e., superposition and/or division) together with the evaluations of beams generated through LMs, ASTAs, non-steering (experiments) [23]. The geometries of PSFs and sources depend on focus methods and apodization functions such as rectangular, power and Gaussian functions etc. The spectra frequency division and coherent superposition respectively decreased and increased bandwidths (i.e., spatial resolutions). In refs. [8,13], such evaluations were performed for quasi-LM that was achieved by disregarding low lateral frequency spectra for non-steering. Although generated low frequency waves can also be evaluated in a frequency domain, in this report, generated US beams were evaluated. Super-resolution was also performed, for instance, on LM with steered plane wave transmissions and Gaussian apodization [24] (Although a narrow bandwidth was obtained, multidimensional Doppler method yields rather accurate displacement vector measurement [3] with fewer calculations than MAM [4]). Alternatively, the generated mechanical and thermal sources were evaluated by estimating multidimensional autocorrelation functions on received echo signals. For high intensity focus US transmission (treatment and radiation force), a concave transducer (simulation) [24] and a linear array type transducer (agar phantom experiment) [23] were used with echo imaging (LM, single beam beamforing, etc.). The above-mentioned speckle reduction was also performed (agar phantom). For agar phantom experiments, the same echo data were used as synthetic aperture echo data of ref. [8,13] for lateral compression case; and as those of ref. [28] for axial compression case (nominal US frequency, 7.5 MHz).

Results

As mentioned above, the disregarding low axial frequency spectra was particularly effective for parabolic apodization. Although the disregarding axial spectra did not increase measurement accuracy (only LM results for a lateral compression case are shown in Figure 2), the displacement calculation speed increased. With respect to the axial moment, 7 MHz and the lowest frequency, about 3.1 MHz, the low cutoff frequency up to about 4.68 to 5.85 MHz achieved the high measurement accuracy. When using plane wave transmissions and/or rectangular apodization, the degradation of measurement accuracy occurred at lower cutoff frequencies (omitted).

Measurements (lateral strains) obtained using horizontal two divisions of spectra are shown in Figure 3a (a lateral compression case), i.e., by using weighted over-determined systems generated by the spectra division with different boundary frequency fb (Figure 3a). Non-divided raw spectra were also used to increase the measurement accuracy, whereas no used cases of raw spectra are omitted (here). Weights are determined by Ziv-Zakai Lower Bound and/or energy of spectra (Figure 3b). The accuracy obtained using the raw spectra solo is also shown. The slight effectiveness was confirmed for the measurement obtained using fb = 7.0 MHz (lower than the moment in the beam direction, 7.6 MHz). Although the weighting was also performed at the respective measurement positions similarly to that performed in refs. [26,27], the

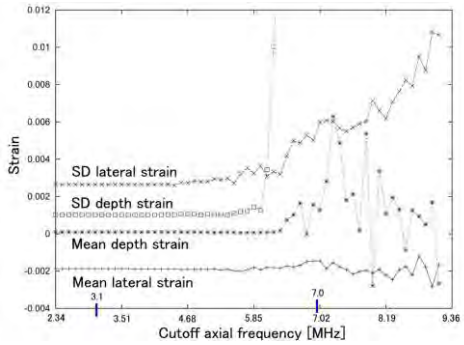

Figure 2. For parabolic LM, measurement accuracies of axial and lateral strains (agar lateral compression [8,13]) vs cutoff axial frequency. Moment, 7.0 MHz; the lowest frequency, about 3.1 MHz.

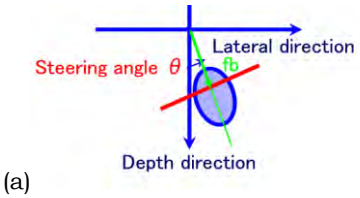

(a)

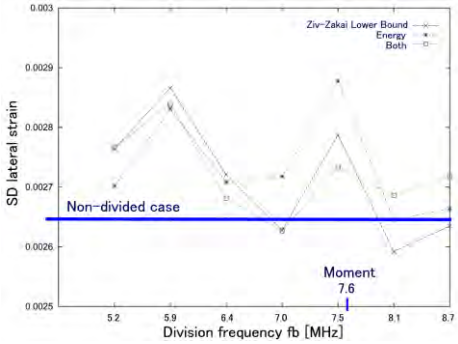

(b)

Figure 3. (a) Horizontal two divisions of spectra. (b) Measurements (lateral strains) on agar phantom using weighted over-determined systems generated by the spectra division [(a)] with different boundary frequency fb (Non-divided raw spectra was also used). Weights are determined by Ziv-Zakai Lower Bound and/or energy of spectra. The accuracy obtained using the raw spectra solo is also shown.

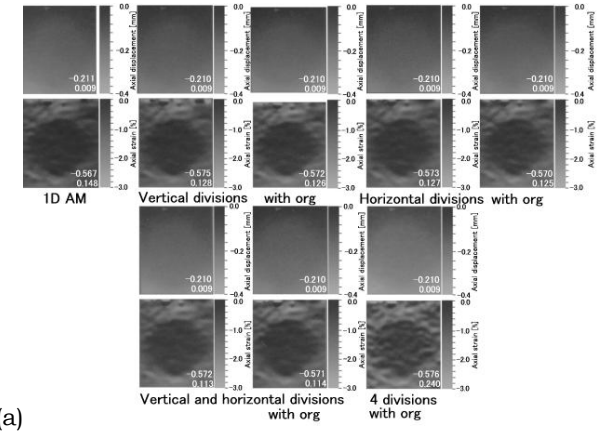

(a)

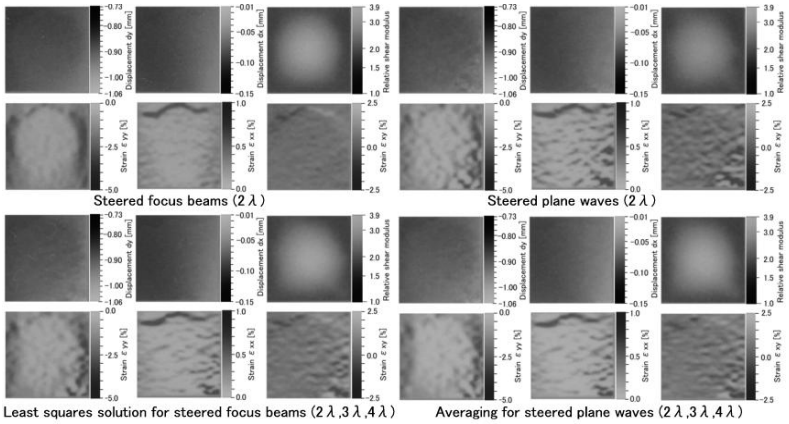

(b)

Figure 4. Over-determined systems (reviews of presented slides at the 10th conf. [13]) (a) for axial strain measurement with non-steering (axial compression) and (b) measurements (lateral compression) of strain tensor and shear moduli with LM with steered beams (lateral wavelengths, 2λ, 3λand 4λ). See also statistics (Figures 2 in ref. [13]).

measurement accuracy decreased (omitted). Any more vertical and horizontal divisions (> totally, 3) also decreased the measurement accuracy (omitted). The images obtained are also omitted, and instead, images obtained through other beamforming such as non-steering and LMs with plane wave transmissions are shown in Figure 4 (i.e., images shown at the 10th conf. [13]). See also the corresponding statistics shown in Figures 2a and 2b in ref. [13]. The combinational use with non-steering (ie, 0 degree and lateral wavelength, $^{\infty}\lambda$) was effective for plane wave transmissions (steered and non-steered cases) and not for spherical focus transmissions [13]. In addition, for low echo SNR, averaging of measurements yielded more accurate results than the least squares solution [13]. Spectra division performed on superposed echo data are also omitted here. These results will also be reported in detail elsewhere.

Next, estimated PSFs (generated beams), and thermal and mechanical sources are shown for the coherent superposition and/or spectra frequency division. Weighting the spectra also allows for improving the image quality. Figure 5 shows for parabolic LMs with plane wave transmissions the effectiveness of the superposition of raw spectra (lateral wavelengths, 2λ, 3λand 4λ). For LM, the combination with 2λ and 3 λ was effective in that the lateral bandwidth increased and the crossed plane waves with only 2λdisappeared (spatial resolution increased). However, such combination decreased the lateral frequency, and therefore the measurement accuracy of lateral displacement or displacement vector decreased (omitted). See also the image obtained by the combination with 4λ. For comparison, the combination with non-steering ($^{\infty}\lambda$) is also performed. Although the combination yielded larger lateral bandwidth and frequency than the non-steering solo, a lower measurement accuracy was obtained than the combined LM with the highest lateral frequency solo similarly [23] (omitted). Similar results were obtained for non-steered plane wave transmissions with the same reception steering angle (obtained wavelengths, 4λ, 6λ, 8λand $^{\infty}\lambda$, omitted) [23]. These results will be reported in detail elsewhere. For spherical focus transmission, results [23] are presented later in the cases where high intensity focus US treatment and/or ARFI are performed. For low lateral spatial resolution Gaussian LM with steered plane wave transmissions, super-resolution was performed. In this report, the target was set to the high spatial resolution parabolic LM with spherical focusing (Figure 6). The real and imaginary spectra components were weighted such that the spectra

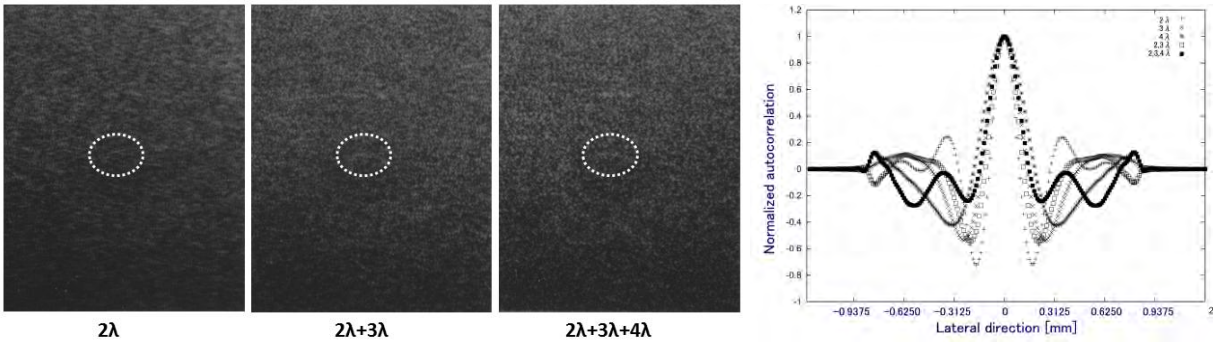

Figure 5. For parabolic LM with plane wave transmissions, coherent superposition: 2λ, 3λand 4λ.

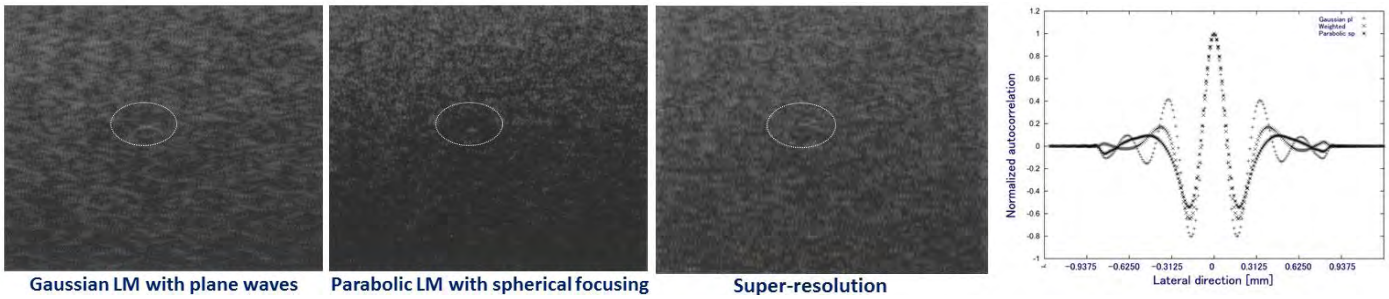

Figure 6. Super-resolution imaging for Gaussian LM with steered plane wave transmissions (target, parabolic LM).

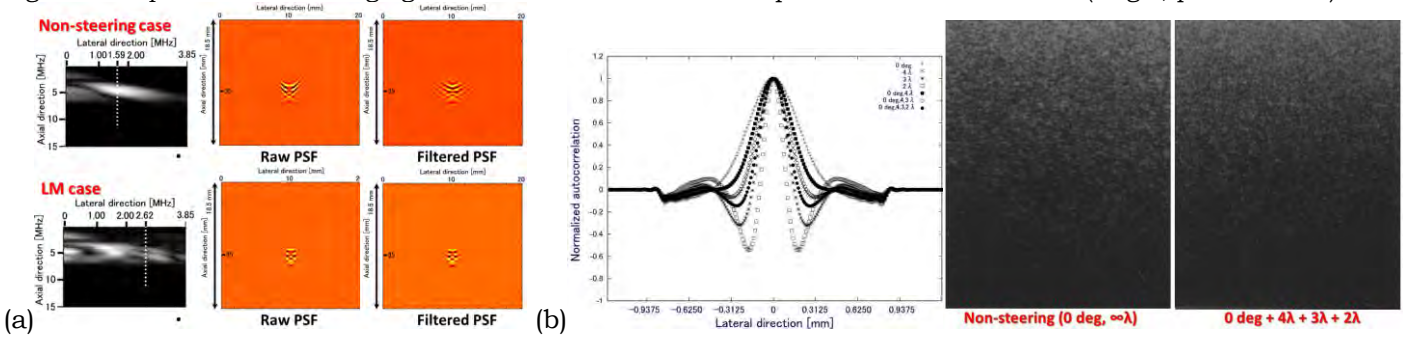

Figure 7. For HIFU, ARFI and conventional imaging, (a) improvement in PSF by filtering (simulations). LM (crossed angle, 10 degrees) and non-steering cases using concave-type transducers (5MHz). (b) For agar phantom [8,13], the increase in a lateral spatial resolution performed by superposition of non-steering and steered beams obtained using a linear array-type transducer with parabolic apodization. Simultaneous echo imaging is also performed.

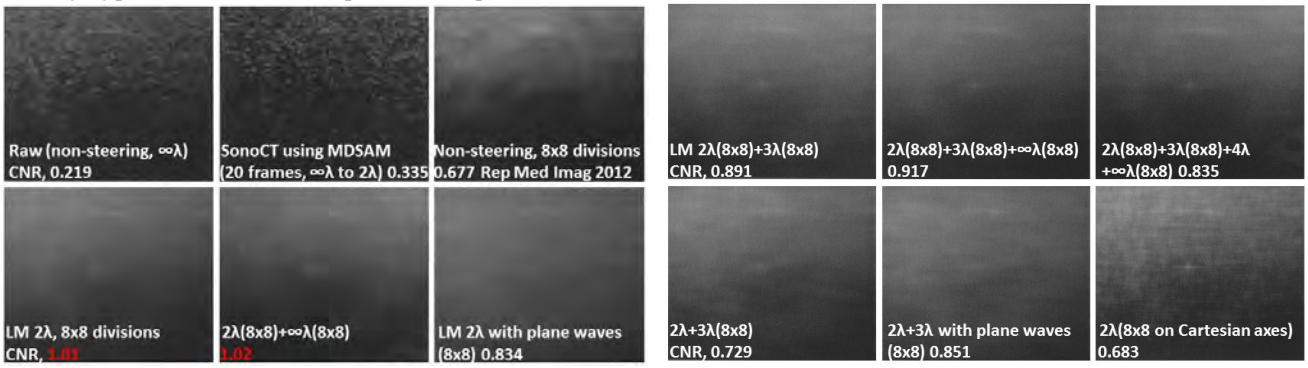

Figure 8. Speckle reduction using spectra division on various raw spectra and coherently superposed spectra. Spectra division is more effective for LM 2λthan for non-steering (∞λ). Incoherent superposition with ∞λ result increases CNR. However, ineffective with the superposition with other larger λ (ie, 3λand 4λ). Superposition should be performed incoherently rather than coherently. Plane wave transmissions decrease CNR (2λ), however, effective with the superposition with 3λ. 64 (8x8) divisions should be performed in the respective beam directions and the orthogonal directions rather than on the Cartesian Coordinate axes.

became same at the respective frequencies. The bandwidth with larger spectra than the maximum spectra multiplied by 10^{-6} (threshold) were weighted. Although the spatial resolution increased (see also changes in PSF), the measurement accuracy decreased due to the amplification of noise with the low echo SNR frequency. For an accurate measurement, the threshold must be set smaller. Also the super-resolution was performed on other beamforming. Such results will be reported in detail elsewhere.

The shapes and magnitudes of PSFs, and thermal and mechanical sources were also controlled using

filtering in a frequency domain. In simulations (Field II [29]), only two concave-type transducers (5 MHz) were used for LM with a crossed angle, 10 degrees (Figure 7a). Also the single non-steering case is shown. By disregarding the spectra properly, the shapes of PSFs became circular. This will lead to the improvement in an image quality and displacement vector measurement. For agar phantom [8,13], increase in a lateral spatial resolution was performed by superposing of non-steered and steered echo data obtained using a linear array-type transducer (Figure 7b). Spherical focusing was performed, and simultaneous echo imaging was also performed (see also PSFs). Recall the effects on measurement accuracy mentioned above.

In addition, for speckle reduction, we performed incoherent superposition with plural divisions on raw plural spectra and/or coherent superposition (see Figure 8). The spectra division yielded higher contrast-to-noise ratios (CNRs) than SonoCT obtained with MDSAM, a non-steering case and steered single beam case.

Conclusions

For the above-mentioned respective purposes, mixing and/or division were performed with respect to the spectra obtained using LMs, ASTAs and non-steering. Disregarding the low axial frequency spectra was also performed to increase the displacement calculation speed. Signal separations and generations of quasi-beams were also possible. The PSF (US beams), ARFI and HIFU sources generated were evaluated using an autocorrelation function for the coherent superposition and/or spectral frequency division (rectangular, power and Gaussian apodizations). The geometries were also controlled using filtering in a frequency domain. Super-resolution was also performed for LM. The generated beams were evaluated in the frequency domain. Additionally, optimized beamforming can also be performed. The PSF estimated will also be used for mechanical and thermal reconstructions [17,18] (geometry and relative magnitude can be used). For the use of nonlinearity and harmonic components for imaging and treatment, the US beamforming and generation of the low frequency wave should be performed with simultaneous or successive plural transmissions or vibrations, although the signal processing methods used in this report can also be used approximately in any cases. Incoherent superposition with plural spectra divisions was also effective for speckle reduction. All these can also be performed microscopically and will be reported in detail elsewhere.

References

[1] C. Sumi, T. Noro, A. Tanuma: IEEE Trans. on UFFC, Vol. 55, pp. 2607–2625, 2008.
[2] C. Sumi: Technical report of Japan Society of Ultrasound Medicine, p. 37–40, Dec 2002 (in Japanese).
[3] C. Sumi, A. Tanuma: Jpn J Appl Phys, Vol. 47(5B), pp. 4137–4144, 2008.
[4] C. Sumi: IEEE Trans. on UFFC, Vol. 55, pp. 24–43, 2008.
[5] C. Sumi, Y. Takanashi and K Ichimaru: Reports in Medical Imaging, Vol. 5, pp. 23–50, 2012.
[6] C. Sumi, K. Ichimaru, Y. Shinozuka: Reports in Medical Imaging, Vol. 4, pp. 47-66, 2011.
[7] C. Sumi: Reports in Medical Imaging, Vol. 3, pp. 45-59, 2010.
[8] C. Sumi, Y. Ishii: Reports in Medical Imaging, Vol. 5, 2012 (in press).
[9] C. Sumi: IEEE Trans. on UFFC, Vol. 52, pp. 1670–1689, 2005.
[10] C. Sumi: Japanese Patent 4260523, Apr 30, 2009 (Application, Apr 25, 2002); US Patent 7,775,980 B2, Aug 17, 2010 (Application, Dec 23, 2002); US Patent 7,946,180 B2, May 24, 2011.
[11] C. Sumi: Japanese patent 4731863. Apr 28, 2011 (Application Oct 15, 2003); Japanese patent publication JP-P2007-152074A. Jun 21, 2007 (Application Jan 21, 2005); US Patent 8,211,019 B2, Jul 3, 2012 (Application, Jan 18, 2006).
[12] C. Sumi, Y. Komiya, S. Uga: Jpn J Appl Phys, Vol. 48(7B), 07GJ06, 2009.
[13] C. Sumi et al: Proc (p. 73) and full version proc of 10th Int Tissue Elasticity Conf, 2011.
[14] C. Sumi: Proc of 1st Int Tissue Elasticity Conf, p. 23, 2002.
[15] C. Sumi, H. Matsuzawa: J Med Ultrasonics, Vol. 34, pp. 171–188, 2007 (in English).
[16] C. Sumi: Japanese Patent Application P2003-210406A (Application, Jan 18, 2002).
[17] C. Sumi, S. Suekane: Thermal Med, Vol. 25(4), pp. 89-103, 2009.
[18] C. Sumi, H. Kanada, Y. Takanashi: Thermal Med, Vol. 26(1), pp. 31-40, 2010.
[19] C. Sumi, Y. Saijo: Shear modulus microscopy using displacement vector measurement, Full version proc of 7th Int Tissue Conf, 2008.
[20] T. Sugimoto, S. Ueha, K. Itoh: Jpn J Med Ultrasonics, 20: 277-283, 1993 (in Japanese).
[21] J. J. Dahl et al: IEEE Trans. UFFC, Vol. 54, pp. 301-312, 2007.
[22] J. Bercoff J, M. Tanter, M. Fink: IEEE Trans. UFFC, Vol. 51, pp. 396-409, 2004.
[23] C. Sumi, Y. Ishii, Y. Hirabayashi: IEICE Tech Rep, Vol. US2012-4, pp. 33-38, 2012 (in Japanese).
[24] C. Sumi, Y. Ishii: IEICE Tech Rep, Vol. US2012-9, pp. 13-19, 2012 (in Japanese).
[25] I. Cespedes, J. Ophir, K. Alam: IEEE Trans. on UFFC, Vol. 44, pp. 220–225, 1997.
[26] C. Sumi: IEEE Trans. on UFFC, Vol. 55, pp. 297-307, 2008.
[27] C. Sumi, T. Itoh: Ultrasonics, Vol. 49, pp. 459-465, 2009.
[28] C. Sumi, T. Ebisawa: Acoust Sci Tech, Vol. 30, pp. 124–131, 2009.
[29] J. A. Jensen: Proc of Med Biol Eng Comp, 10th Nordic-Baltic Conf Biomed Imag, pp. 351–353, 1996.